Local distortion driven magnetic phase switching in pyrochlore $Yb_2(Ti_{1-x}Sn_x)_2O_7$

Yuanpeng Zhang,[1] Zhiling Dun,[2] Yunqi Cai,[2] Chengkun Xing,[3] Qi Cui,[2] Naveen Kumar Chogondahalli Muniraju,[4,5,6] Qiang Zhang,[1] Yongqing Li,[2] Jinguang Cheng,[2,*] and Haidong Zhou[3,†]

[1]*Neutron Scattering Division, Oak Ridge National Laboratory, Oak Ridge, Tennessee 37831, USA*

[2]*Institute of Physics, Chinese Academy of Sciences, Beijing 100190, China*

[3]*Department of Physics and Astronomy, University of Tennessee, Knoxville, Tennessee 37996, USA*

[4]*Forschungszentrum Jülich GmbH, Jülich Centre for Neutron Science (JCNS), Forschungszentrum Jülich, D-52425 Jülich, Germany*

[5]*Chemical and Engineering Materials Division, Oak Ridge National Laboratory, Oak Ridge, Tennessee 37831, USA*

[6]*Institute of Physics, Bijenička cesta 46, 10000 Zagreb, Croatia*

(Received 5 October 2023; revised 19 February 2024; accepted 13 March 2024; published 9 April 2024)

While it is commonly accepted that the disorder induced by magnetic ion doping in quantum magnets usually generates a rugged free-energy landscape resulting in slow or glassy spin dynamics, the disorder/distortion effects associated with nonmagnetic ion sites doping are still illusive. Here, using AC susceptibility measurements, we show that the mixture of Sn/Ti on the nonmagnetic ion sites of pyrochlore $Yb_2(Ti_{1-x}Sn_x)_2O_7$ induces an antiferromagnetic ground state despite both parent compounds, $Yb_2Ti_2O_7$ and $Yb_2Sn_2O_7$, order ferromagnetically. Local structure studies through neutron total scattering reveals the local distortion in the nonmagnetic ion sites and its strong correlation with the magnetic phase switching. Our study demonstrates the local distortion as induced by the nonmagnetic ion site mixture could be a new path to achieve magnetic phase switching, which has been traditionally obtained by external stimuli such as temperature, magnetic field, pressure, strain, light, etc.

DOI: 10.1103/PhysRevB.109.144407

I. INTRODUCTION

The complex interplay between various degree of freedom in frustrated quantum systems enables rich physics involving complex ground states and exotic excitations [1,2]. The balancing between those weak interaction terms in the Hamiltonian (long-range dipolar interactions, exchange interaction beyond the nearest neighboring, site disorder, lattice distortions, etc.) and the frustration could determine the coordination in the phase diagram [3–6]. Exploring such a complex interplay thus becomes critical in terms of understanding the formation of those exotic states such as the quantum spin liquid (QSL) state where the long range magnetic ordering is completely suppressed by frustration and the quantum fluctuation yields strong dynamics even at zero temperature. Though the QSL state of matter (e.g., the non-Abelian anyons in 2D QSL) hosts promising applications in practice such as the error-proof quantum computation [7–9] and high temperature superconductivity [10–12], the identification of the true QSL states among possibilities is challenging. Typically, for the parent compound $Yb_2Ti_2O_7$ of the samples to be studied in this report, it had long been believed that the quantum fluctuation is associated with the QSL physics [6,13–15]. However, more recent studies by A. Scheie *et al.* revealed that it is in fact the ferro- (FM) and antiferromagnetic (AFM) phase competition that accounts for the quantum fluctuation [16–18]. This infers that the phase switching between FM and AFM should be paid serious attention in the studies of quantum fluctuations in both $Yb_2Ti_2O_7$ and its derivative compounds.

The lattice degree of freedom, encompassing chemical order/disorder and lattice/sublattice distortion, is crucial in determining the magnetic phase diagram. For example in pyrochlore systems, which are the main focus of the current report, extensive research has been conducted on the effects of disorder related to magnetic species, including those diluted [19–23] or stuffed [24–27] pyrochlores. In such systems, the chemical order/disorder resulting from doping can introduce randomness into the magnetic Hamiltonian, thereby impacting the magnetic phase diagram. Following such studies, there are recently emerging interest in exploring the nonmagnetic species doping on the nonmagnetic sites in frustrated quantum systems. Several notable examples are $YbMgGaO_4$ (YMGO) [28–32], $Sr_3CuTa_2O_9$ (SCTO) [33], $Sr_2Cu(Te_{1-x}W_x)O_6$ (SCTWO) [34–36], etc. Compared to the magnetic species doping, nonmagnetic doping on nonmagnetic sites has a limited direct involvement in magnetic coupling. As a result, the disorder effect induced by nonmagnetic doping is not expected to play as significant a role in interplaying with the magnetic coupling, which provides opportunities to better understand the separate influences of disorder and distortion. However, the practical impact of nonmagnetic doping on nonmagnetic sites upon the magnetic phase diagram remains complex and not fully understood. Further, although excessive theoretical work has provided clear indication for the impact of local structural distortion,

*jgcheng@iphy.ac.cn
†hzhou10@utk.edu

via the spin-lattice coupling effect, upon the magnetic states and spin ordering [37–43], direct experimental probing of the local structural variation and its link to the magnetic coupling, especially in the pyrochlore systems, is still lacking. To the best of our knowledge, there is only limited experimental work focusing on the spin-lattice coupling effect in pyrochlore systems from the local perspective, like the report by P. M. Thygesen, *et al.* demonstrating the local orbital dimerization of Jahn-Teller active Mo^{4+} ions instead of random compositional or site disorder drives the spin-glass state in $Y_2Mo_2O_7$ [44]. More relevant experimental efforts, though still limited, were mainly from the average long-range structure perspective [24,45–47]. However, while the local distortion could be extracted from conventional Bragg diffraction, the local and short-range probe could provide unique pathway and different angle to such explorations, as is already demonstrated by the work on the herbertsmithite and barlowite QSL candidate systems [48–53]. In this report, we are trying to focus on the $Yb_2Ti_2O_7$ pyrochlore system and exploring the effect of the Sn doping on the nonmagnetic Ti sites. The magnetic susceptibility measurement was employed to study the magnetic phase switching and neutron total scattering combined with the reverse Monte Carlo (RMC) modeling was utilized to explore the local distortion and its potential link to the magnetic phase switching.

II. NEUTRON AND X-RAY DIFFRACTION

For comparison, we synthesized both $Yb_2(Ti_{1-x}Sn_x)_2O_7$ and $Yb_2(Ti_{1-x}Ge_x)_2O_7$ samples and used neutron powder diffraction (NPD) and synchrotron x-ray diffraction(SXRD) to characterize their lattice structures. Figure 1(a) shows the refinement for the NPD data of $Yb_2(Ti_{0.6}Sn_{0.4})_2O_7$ measured at room temperature using the POWGEN diffractometer [55]. The data could be well fitted by the $Fd\bar{3}m$ pyrochlore structure. Though minor contribution from impurity phase could be observed (e.g., ∼2.8 Å), the impact upon the major phase refinement should be ignorable, for both the average structure analysis and the local structure analysis below. The NPD data for several other Sn and Ge doped samples was also refined (not shown here), which all exhibits pure pyrochlore structure. As summarized in Fig. 1(b), the lattice parameter a decreases from $Yb_2Sn_2O_7$ to $Yb_2Ti_2O_7$ and then $Yb_2Ge_2O_7$ for all doped samples. This is reasonable since the lattice parameter is strongly related to the ionic radius of the (Sn/Ti/Ge) site, and therefore the Sn sample has the largest lattice parameter, Ti sample the second, and Ge sample the smallest. We further used $\rho = d_{\text{Yb-O2}}/d_{\text{Yb-O1}}$ and the Yb-O2-Yb angle to characterize the axial distortion of the YbO_8 polyhedra, here $d_{\text{Yb-O1}}$ represents the bond length for the six longer Yb-O1 bonds in the plane perpendicular to the ⟨111⟩ axis and $d_{\text{Yb-O2}}$ represents the bond length for the two shorter Yb-O2 bonds along the ⟨111⟩ axis. As shown in Fig. 1(c), again, both of them decrease linearly, without abrupt change.

III. AC SUSCEPTIBILITY

Figure 2 shows the AC susceptibility measured at different DC magnetic fields for $Yb_2(Ti_{1-x}Sn_x)_2O_7$ and

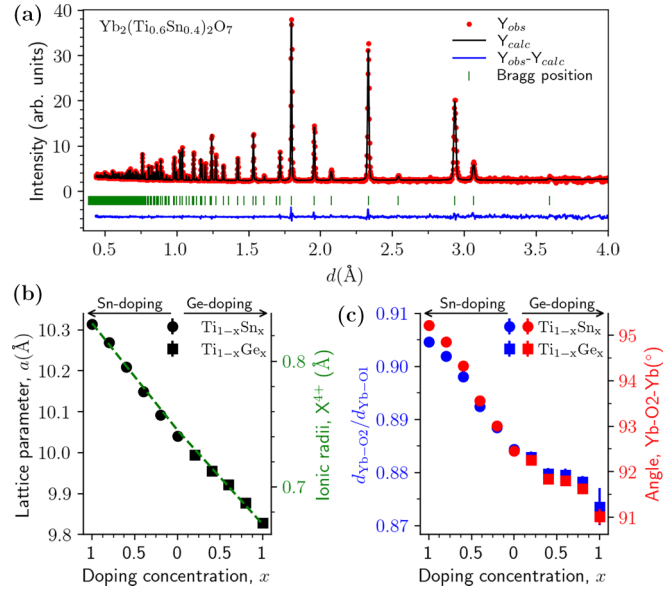

FIG. 1. Average structure of $Yb_2(Ti_{1-x}Sn_x)_2O_7$ and $Yb_2(Ti_{1-x}Ge_x)_2O_7$. (a) Neutron powder diffraction pattern (red circles) for $Yb_2(Ti_{0.6}Sn_{0.4})_2O_7$ measured at 300 K with the central wavelength of 1.5 Å on POWGEN diffractometer. The solid black line is the Rietveld refinement using [54]. Solid blue line at the bottom of the panel shows the difference curve. The Bragg peaks are marked with green markers. (b) The doping concentration dependence of the lattice parameter. (c) The doping level dependence of the ratio between the two different Yb-O bond lengths and the Yb-O2-Yb angle.

$Yb_2(Ti_{1-x}Ge_x)_2O_7$. For all samples, the data at zero field exhibits a peak, which represents the long range magnetic ordering at T^*, and such a peak shows obviously shift under applied DC fields. As demonstrated in Ref. [56], the field dependence of AC susceptibility can be used as a convenient tool to identify the nature of a long-range magnetic ordering, i.e., the ferromagnetic (FM) ordering temperature will shift to higher temperatures with increasing DC field due to the contribution of domain magnetization while the antiferromagnetic (AFM) ordering temperature will show an opposite DC field dependence.

The field dependence of T^* for each doping level was summarized in Fig. 3(a). The data shows (i) for $Yb_2Ti_2O_7$ and $Yb_2Sn_2O_7$, the T^* increases with increasing field, which is consistent with the fact that both samples have a splayed ferromagnetic (SF) ground state; (ii) for $Yb_2Ge_2O_7$, the T^* decreases with increasing field, which is consistent with its AFM ground state [56–58]; and (iii) for all Sn- and Ge-doped samples except $Yb_2(Ti_{0.8}Sn_{0.2})_2O_7$, the T^* decreases first with increasing field and then increases while the field surpasses a critical value H_c. This indicates that as soon as Sn and Ge are doped, certain volume of AFM phase is introduced. This AFM order should be in long range nature since it dominates the bulk magnetism at low fields. With $H > H_c$, the sample comes back to ferromagnetic or is fully polarized; (iv) for $Yb_2(Ti_{0.8}Sn_{0.2})_2O_7$, it has ferromagnetic ground state since its T^* monotonically increases with increasing field. Further, the frequency dependent AC data are presented in

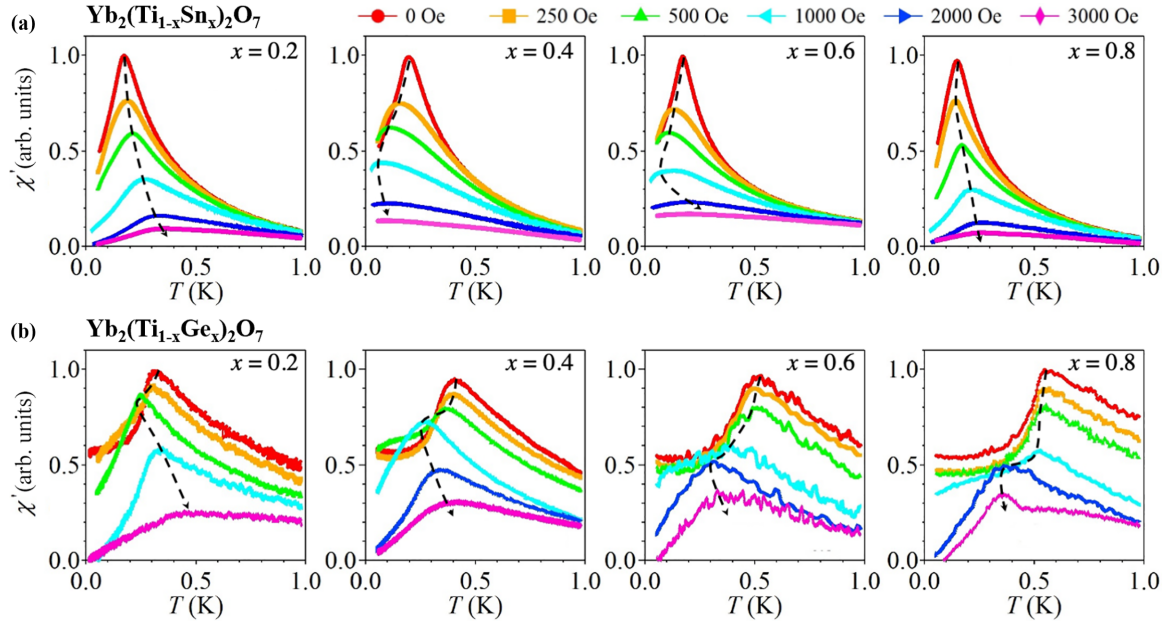

FIG. 2. AC susceptibility. (a) Real part of AC susceptibility measured under different DC magnetic fields in the arbitrary unit (arb. units) for $Yb_2(Ti_{1-x}Sn_x)_2O_7$ with $x = 0.2$, 0.4, 0.6, and 0.8. (b) Similar data for $Yb_2(Ti_{1-x}Ge_x)_2O_7$ with $x = 0.2$, 0.4, 0.6, and 0.8. The used AC frequency is 3317 Hz for the Sn-doped system and 331 Hz for the Ge-doped system with a magnitude of 5 Oe. Dashed arrows indicate the evolution of the peak's position with increasing DC fields.

Ref. [59]—the AC susceptibility peak position shows no obvious frequency dependence between the data measured with $H = 331\,Hz$ and $H = 3317\,Hz$, thus ruling out the spin glass state possibility.

IV. MAGNETIC PHASE DIAGRAM

Accordingly, a magnetic phase diagram of T^* and H_c for $Yb_2(Ti_{1-x}Sn_x)_2O_7$ and $Yb_2(Ti_{1-x}Ge_x)_2O_7$ is summarized in Fig. 3(b). For Ge-doped samples, both T^* and H_c monotonically increase with increasing Ge-doping level. On the other hand, for Sn-doped samples, (i) while the T^* generally decreases with increasing Sn-doping level, it exhibits a dome around $x = 0.5$; (ii) the H_c first increases with increasing Sn-doping level, peaks at $x = 0.5$, and thereafter decreases.

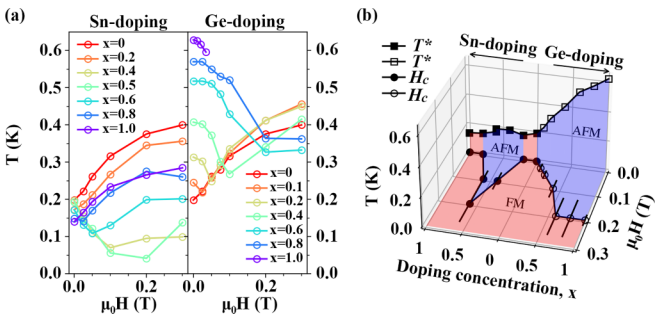

FIG. 3. Magnetic phase diagram. (a) The field dependence of the magnetic ordering temperature T* for $Yb_2(Ti_{1-x}Sn_x)_2O_7$ and $Yb_2(Ti_{1-x}Ge_x)_2O_7$ with different doping concentration. (b) Magnetic phase diagram as a function of the doping concentration x, temperature T, and external DC field $\mu_0 H$. Red and blue regions represent the FM and AFM phases, respectively. Data points for $Yb_2Ti_2O_7$, $Yb_2Sn_2O_7$, and $Yb_2Ge_2O_7$ are from Dun *et al.* [56].

The evolution of T^* and H_c in the Ge-doped samples is expected. The magnetic ground states of Yb-pyrochlores are determined by the ratio among the anisotropic exchange interactions [57,60,61]. Unlike $Yb_2Ti_2O_7$, $Yb_2Ge_2O_7$ orders antiferromagnetically in the Γ_5 manifold [58]. From the point view of chemical pressure effect, with increasing the Ge-doping level in $Yb_2(Ti_{1-x}Ge_x)_2O_7$, the lattice parameter decreases monotonically and gradually tunes the balance of anisotropic exchange interactions that drives the system towards the AFM Γ_5 phase from the SF phase [57,58]. Alternatively, if we assume that the phase coexistence in Ge-doped samples is similar to that of $Yb_2Ti_2O_7$, then the H_c could be related to the strength of the exchange interaction of the AFM phase since the larger the H_c is, the more difficult to polarize the system. Therefore, the evolution of H_c in Fig. 3(b) means a monotonic increase of the AFM interaction in $Yb_2(Ti_{1-x}Ge_x)_2O_7$, consistent with the SF and AFM phases in $Yb_2Ti_2O_7$ and $Yb_2Ge_2O_7$, respectively.

However, although we cannot determinate whether it is the ψ_2 or ψ_3 phase of the Γ_5 manifold, the appearance of the long range AFM order in $Yb_2(Ti_{1-x}Sn_x)_2O_7$ is surprising. Since both $Yb_2Ti_2O_7$ and $Yb_2Sn_2O_7$ have the SF ground state, an AFM ground state should not be expected for Sn-doped samples from the view of chemical pressure effects. Even if there is still magnetic phase coexistence [16], it is puzzling to observe this nonmonotonic change of H_c in $Yb_2(Ti_{1-x}Sn_x)_2O_7$.

V. TOTAL SCATTERING

The total scattering signal contains both the Bragg peaks and the diffuse scattering contribution. The diffuse scattering part, which is usually taken as the background and thus

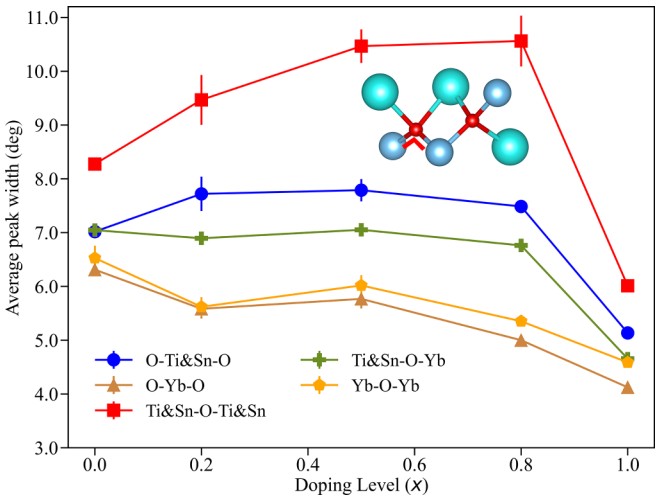

FIG. 4. Local distortion as characterized by various local bond angles, as extracted from the RMC resulted configuration. The inset is an illustration for the local geometry involving the critical triplet angle–Ti and Sn-O-Ti and Sn. Yb → cyan, Ti and Sn → blue, O → red. Error bar was estimated via running 15 repeated RMC modeling on three different computers (5 on each), followed by the same bond angle calculation. The variation trend as the function of the doping level is preserved considering the uncertainty level, regarding the discussion in the context.

subtracted off in conventional Bragg peaks analysis, in fact provides unique access to the local structure. Although both the Bragg peaks and total scattering data would yield information about local distortions, the former is based on *the distance between average positions* whereas the latter is based on *the average of distances ensemble*. Therefore, the local probe via total scattering data could provide access to the local structural variation that is inaccessible through the conventional Bragg analysis. Here, we collected neutron total scattering data on POWGEN for the series of $Yb_2(Ti_{1-x}Sn_x)_2O_7$ samples and performed the reverse Monte Carlo (RMC) [62,63] modeling to extract the local structure (see the Supplemental Material [59], including references [62–65]). A $10 \times 10 \times 10$ supercell containing 88 000 atoms could be constructed from the RMC modeling and the following statistical calculation could be performed to extract the key structural aspects. Typically, here we focused on the various bond angles involving both the Yb, Ti/Sn, and O atoms – from the RMC resulted configuration, a statistical distribution of various triplet angles could be obtained [59]. Further, the width of the triplet angles distribution could be extracted through a Gaussian peak fitting, which indicates the dispersiveness of the bond angle and thus infers the significance of the local distortion. In another word, a larger peak width value indicates a wider distribution of the triplet angle, which further infers a larger degree of the relevant local distortion. The results are presented in Fig. 4. No abrupt change as the function of the doping level could be observed except for the Ti and Sn-O-Ti and Sn triplet (see the inset of Fig. 4). Further, the trend of the observed variation of the Ti and Sn-O-Ti and Sn triplet angle as the function of the doping level tends to be consistent with the magnetic phase switching behavior as the doping level varies. The results here indicate the non-magnetic-site involved local distortion is enhanced as the result of the doping and a phenomenal link could be observed between such an enhancement of local distortion and the magnetic phase switching behavior. This is an interesting finding since one would expect the magnetic species involved sublattice distortion to be directly linked to the magnetic coupling. According to various reports by K. A. Ross and others [6,15,66–68], the nearest-neighbor (NN) interaction dominates the magnetic coupling in $Yb_2Ti_2O_7$. If assuming the NN interaction stays dominant in the doped $Yb_2(Ti_{1-x}Sn_x)_2O_7$ system, the nonmagnetic doping is not expected to introduce randomness along the magnetic interaction pathway. In such a situation, the magnetic phase switching associated with the nonmagnetic doping should be considered as being caused by the local distortion. Fundamentally, the electron redistribution associated with the local nonmagnetic sublattice distortion [69–72] could indirectly impact the magnetic coupling across the Ti-O-Ti exchange pathway, through the bridging O atoms as illustrated in the inset of Fig. 4. Such a scenario falls in line with various theoretical studies for the spin-lattice coupling in pyrochlore systems. For example, through many-body quantum-chemical calculations, N. Bogdanov *et al.* showed the magnetic interactions and ordering in $Cd_2Os_2O_7$ are crucially dependent on the local geometrical features [41]. H. Shinaoka, *et al.* showed the coupling of spin-glass transitions to local lattice distortions on pyrochlore lattices via Monte Carlo simulation [38]. Also using Monte Carlo simulation, K. Aoyama *et al.* revealed a lattice distortion induced spin ordering in the breathing pyrochlore lattice [37].

As a final remark, it is important to highlight that our conclusion regarding the causal relationship between local distortion and magnetic phase switching is based on the assumption that the NN interaction is still dominant in the doped $Yb_2(Ti_{1-x}Sn_x)_2O_7$ system. However, the possibility of the NN interaction being altered to extend to the next nearest neighbor interaction does exist. As reported in the SCTWO system, the W doping on the Te sites was found to alter the magnetic interactions from nearest-neighbor (NN) to next-nearest-neighbor (NNN) coupling, which further induces randomness in the Hamiltonian and alters the magnetic ground state [35]. As such, further experimental and theoretical explorations on the doped $Yb_2(Ti_{1-x}Sn_x)_2O_7$ system are needed – magnetic interaction beyond the nearest neighbor needs to be inspected and its effect on the magnetic phase diagram should be studied.

ACKNOWLEDGMENTS

We thank Martin Mourigal and Itamar Kimchi for helpful discussion. J.C. is supported by the National Natural Science Foundation of China (12025408, 11874400, 11921004), the Key Research Program of Frontier Sciences of CAS(QYZDB-SSW-SLH013), the CAS Interdisciplinary Innovation Team (JCTD-2019-01) and Lujiaxi international group funding of K. C. Wong Education Foundation (GJTD-2020-01). The work at the University of Tennessee is supported by the U. S. Department of Energy under Grant No. DE-SC0020254. Part of the research conducted at SNS was sponsored by the Scientific User Facilities Division, Office of Basic Energy Sciences, US Department of Energy. The following funding is acknowledged: US Department of Energy, Office of

Science (contract No. DE-AC05-00OR22725). This research used birthright cloud resources of the Compute and Data Environment for Science (CADES) at the Oak Ridge National Laboratory, which is supported by the Office of Science of the U.S. Department of Energy under Contract No. DE-AC05-00OR22725. This research used resources of the National Energy Research Scientific Computing Center (NERSC), a Department of Energy Office of Science User Facility using NERSC award BES-ERCAP0027504. We thank Dr. Emil S. Bozin for the discussion about the local structure studies.

[1] J. S. Gardner, M. J. P. Gingras, and J. E. Greedan, Magnetic pyrochlore oxides, Rev. Mod. Phys. **82**, 53 (2010).

[2] J. Shamblin, Z. Dun, M. Lee, S. Johnston, E. S. Choi, K. Page, Y. Qiu, and H. Zhou, Structural and magnetic short-range order in fluorite Yb_2TiO_5, Phys. Rev. B **96**, 174418 (2017).

[3] K. A. Ross, Neutron Scattering studies of the quantum spin ice material Yb_2TiO_7, Ph.D. thesis, McMaster University, 2012.

[4] K. A. Ross, J. P. C. Ruff, C. P. Adams, J. S. Gardner, H. A. Dabkowska, Y. Qiu, J. R. D. Copley, and B. D. Gaulin, Two-dimensional kagome correlations and field induced order in the ferromagnetic XY pyrochlore $Yb_2Ti_2O_7$, Phys. Rev. Lett. **103**, 227202 (2009).

[5] Z. Lu, L. Ge, G. Wang, M. Russina, G. Günther, C. R. dela Cruz, R. Sinclair, H. D. Zhou, and J. Ma, Lattice distortion effects on the frustrated spin-1 triangular-antiferromagnet $A_3NiNb_2O_9$ (A = Ba, Sr, and Ca), Phys. Rev. B **98**, 094412 (2018).

[6] R. Applegate, N. R. Hayre, R. R. P. Singh, T. Lin, A. G. R. Day, and M. J. P. Gingras, Vindication of $Yb_2Ti_2O_7$ as a model exchange quantum spin ice, Phys. Rev. Lett. **109**, 097205 (2012).

[7] M. Banerjee, M. Heiblum, V. Umansky, D. E. Feldman, Y. Oreg, and A. Stern, Observation of half-integer thermal Hall conductance, Nature (London) **559**, 205 (2018).

[8] C. Nayak, S. H. Simon, A. Stern, M. Freedman, and S. Das Sarma, Non-abelian anyons and topological quantum computation, Rev. Mod. Phys. **80**, 1083 (2008).

[9] R. Willett, J. P. Eisenstein, H. L. Störmer, D. C. Tsui, A. C. Gossard, and J. H. English, Observation of an even-denominator quantum number in the fractional quantum Hall effect, Phys. Rev. Lett. **59**, 1776 (1987).

[10] J. R. Chamorro, T. M. McQueen, and T. T. Tran, Chemistry of quantum spin liquids, Chem. Rev. **121**, 2898 (2021).

[11] L. Balents, Spin liquids in frustrated magnets, Nature (London) **464**, 199 (2010).

[12] P. W. Anderson, The resonating valence bond state in La_2CuO_4 and superconductivity, Science **235**, 1196 (1987).

[13] L. Savary and L. Balents, Quantum spin liquids: a review, Rep. Prog. Phys. **80**, 016502 (2017).

[14] G. Chen, "Magnetic monopole" condensation of the pyrochlore ice U(1) quantum spin liquid: Application to $Pr_2Ir_2O_7$ and $Yb_2Ti_2O_7$, Phys. Rev. B **94**, 205107 (2016).

[15] K. A. Ross, L. Savary, B. D. Gaulin, and L. Balents, Quantum excitations in quantum spin ice, Phys. Rev. X **1**, 021002 (2011).

[16] A. Scheie, J. Kindervater, S. Zhang, H. J. Changlani, G. Sala, G. Ehlers, A. Heinemann, G. S. Tucker, S. M. Koohpayeh, and C. Broholm, Multiphase magnetism in $Yb_2Ti_2O_7$, Proc. Natl. Acad. Sci. **117**, 27245 (2020).

[17] J. Robert, E. Lhotel, G. Remenyi, S. Sahling, I. Mirebeau, C. Decorse, B. Canals, and S. Petit, Spin dynamics in the presence of competing ferromagnetic and antiferromagnetic correlations in $Yb_2Ti_2O_7$, Phys. Rev. B **92**, 064425 (2015).

[18] J. D. Thompson, P. A. McClarty, D. Prabhakaran, I. Cabrera, T. Guidi, and R. Coldea, Quasiparticle breakdown and spin Hamiltonian of the frustrated quantum pyrochlore $Yb_2Ti_2O_7$ in a magnetic field, Phys. Rev. Lett. **119**, 057203 (2017).

[19] A. Keren, J. S. Gardner, G. Ehlers, A. Fukaya, E. Segal, and Y. J. Uemura, Dynamic properties of a diluted pyrochlore cooperative paramagnet $(Tb_pY_{1-p})_2Ti_2O_7$, Phys. Rev. Lett. **92**, 107204 (2004).

[20] Sheetal, A. Ali, S. Rajput, Y. Singh, T. Maitra, and C. S. Yadav, Emergence of weak pyrochlore phase and signature of field induced spin ice ground state in $Dy_{2-x}La_xZr_2O_7$, x = 0, 0.15, 0.3, J. Phys.: Condens. Matter **32**, 365804 (2020).

[21] S. K. Takahashi, J. Wang, A. Arsenault, T. Imai, M. Abramchuk, F. Tafti, and P. M. Singer, Spin excitations of a proximate Kitaev quantum spin liquid realized in Cu_2IrO_3, Phys. Rev. X **9**, 031047 (2019).

[22] V. Dantas and E. C. Andrade, Disorder, low-energy excitations, and topology in the Kitaev spin liquid, Phys. Rev. Lett. **129**, 037204 (2022).

[23] W.-H. Kao, J. Knolle, G. B. Halász, R. Moessner, and N. B. Perkins, Vacancy-induced low-energy density of states in the Kitaev spin liquid, Phys. Rev. X **11**, 011034 (2021).

[24] K. A. Ross, T. Proffen, H. A. Dabkowska, J. A. Quilliam, L. R. Yaraskavitch, J. B. Kycia, and B. D. Gaulin, Lightly stuffed pyrochlore structure of single-crystalline $Yb_2Ti_2O_7$ grown by the optical floating zone technique, Phys. Rev. B **86**, 174424 (2012).

[25] D. F. Bowman, E. Cemal, T. Lehner, A. R. Wildes, L. Mangin-Thro, G. J. Nilsen, M. J. Gutmann, D. J. Voneshen, D. Prabhakaran, A. T. Boothroyd, D. G. Porter, C. Castelnovo, K. Refson, and J. P. Goff, Role of defects in determining the magnetic ground state of ytterbium titanate, Nat. Commun. **10**, 637 (2019).

[26] G. C. Lau, R. S. Freitas, B. G. Ueland, B. D. Muegge, E. L. Duncan, P. Schiffer, and R. J. Cava, Zero-point entropy in stuffed spin-ice, Nat. Phys. **2**, 249 (2006).

[27] J. S. Gardner, G. Ehlers, P. Fouquet, B. Farago, and J. R. Stewart, Slow and static spin correlations in $Dy_{2+x}Ti_{2-x}O_{7-\delta}$, J. Phys.: Condens. Matter **23**, 164220 (2011).

[28] Y. Li, D. Adroja, P. K. Biswas, P. J. Baker, Q. Zhang, J. Liu, A. A. Tsirlin, P. Gegenwart, and Q. Zhang, Muon spin relaxation evidence for the U(1) quantum spin-liquid ground state in the triangular antiferromagnet $YbMgGaO_4$, Phys. Rev. Lett. **117**, 097201 (2016).

[29] Y. Li, S. Bachus, B. Liu, I. Radelytskyi, A. Bertin, A. Schneidewind, Y. Tokiwa, A. A. Tsirlin, and P. Gegenwart, Rearrangement of uncorrelated valence bonds evidenced by low-energy spin excitations in $YbMgGaO_4$, Phys. Rev. Lett. **122**, 137201 (2019).

[30] Y. Shen, Y.-D. Li, H. Wo, Y. Li, S. Shen, B. Pan, Q. Wang, H. C. Walker, P. Steffens, M. Boehm, Y. Hao, D. L. Quintero-Castro,

L. W. Harriger, M. D. Frontzek, L. Hao, S. Meng, Q. Zhang, G. Chen, and J. Zhao, Evidence for a spinon fermi surface in a triangular-lattice quantum-spin-liquid candidate, Nature (London) **540**, 559 (2016).

[31] J. A. M. Paddison, M. Daum, Z. Dun, G. Ehlers, Y. Liu, M. B. Stone, H. Zhou, and M. Mourigal, Continuous excitations of the triangular-lattice quantum spin liquid $YbMgGaO_4$, Nat. Phys. **13**, 117 (2017).

[32] Y. Shen, Y.-D. Li, H. C. Walker, P. Steffens, M. Boehm, X. Zhang, S. Shen, H. Wo, G. Chen, and J. Zhao, Fractionalized excitations in the partially magnetized spin liquid candidate $YbMgGaO_4$, Nat. Commun. **9**, 4138 (2018).

[33] B. Sana, M. Barik, S. Lee, U. Jena, M. Baenitz, J. Sichelschmidt, S. Luther, H. Kuehne, K. Sethupathi, M. S. R. Rao, K. Y. Choi, and P. Khuntia, Spin-liquid-like state in a square lattice antiferromagnet, arXiv:2304.13116.

[34] W. Hong, L. Liu, C. Liu, X. Ma, A. Koda, X. Li, J. Song, W. Yang, J. Yang, P. Cheng, H. Zhang, W. Bao, X. Ma, D. Chen, K. Sun, W. Guo, H. Luo, A. W. Sandvik, and S. Li, Extreme suppression of antiferromagnetic order and critical scaling in a two-dimensional random quantum magnet, Phys. Rev. Lett. **126**, 037201 (2021).

[35] E. Fogh, O. Mustonen, P. Babkevich, V. M. Katukuri, H. C. Walker, L. Mangin-Thro, M. Karppinen, S. Ward, B. Normand, and H. M. Rønnow, Randomness and frustration in a $S = \frac{1}{2}$ square-lattice Heisenberg antiferromagnet, Phys. Rev. B **105**, 184410 (2022).

[36] H.-D. Ren, T.-Y. Xiong, H.-Q. Wu, D. N. Sheng, and S.-S. Gong, Characterizing random-singlet state in two-dimensional frustrated quantum magnets and implications for the double perovskite $Sr_2CuTe_{1-x}W_xO_6$, Phys. Rev. B **107**, L020407 (2023).

[37] K. Aoyama and H. Kawamura, Spin ordering induced by lattice distortions in classical Heisenberg antiferromagnets on the breathing pyrochlore lattice, Phys. Rev. B **99**, 144406 (2019).

[38] H. Shinaoka, Y. Tomita, and Y. Motome, Spin-glass transition in bond-disordered Heisenberg antiferromagnets coupled with local lattice distortions on a pyrochlore lattice, Phys. Rev. Lett. **107**, 047204 (2011).

[39] T. Haku, K. Kimura, Y. Matsumoto, M. Soda, M. Sera, D. Yu, R. A. Mole, T. Takeuchi, S. Nakatsuji, Y. Kono, T. Sakakibara, L.-J. Chang, and T. Masuda, Low-energy excitations and ground-state selection in the quantum breathing pyrochlore antiferromagnet $Ba_3Yb_2Zn_5O_{11}$, Phys. Rev. B **93**, 220407(R) (2016).

[40] Y.-P. Huang, G. Chen, and M. Hermele, Quantum spin ices and topological phases from dipolar-octupolar doublets on the pyrochlore lattice, Phys. Rev. Lett. **112**, 167203 (2014).

[41] L. Savary and L. Balents, Disorder-induced quantum spin liquid in spin ice pyrochlores, Phys. Rev. Lett. **118**, 087203 (2017).

[42] N. A. Bogdanov, R. Maurice, I. Rousochatzakis, J. van den Brink, and L. Hozoi, Magnetic state of pyrochlore $Cd_2Os_2O_7$ emerging from strong competition of ligand distortions and longer-range crystalline anisotropy, Phys. Rev. Lett. **110**, 127206 (2013).

[43] E. Berg, E. Altman, and A. Auerbach, Singlet excitations in pyrochlore: A study of quantum frustration, Phys. Rev. Lett. **90**, 147204 (2003).

[44] P. M. M. Thygesen, J. A. M. Paddison, R. Zhang, K. A. Beyer, K. W. Chapman, H. Y. Playford, M. G. Tucker, D. A. Keen, M. A. Hayward, and A. L. Goodwin, Orbital dimer model for the spin-glass state in $Y_2Mo_2O_7$, Phys. Rev. Lett. **118**, 067201 (2017).

[45] X. Li, W. M. Li, K. Matsubayashi, Y. Sato, C. Q. Jin, Y. Uwatoko, T. Kawae, A. M. Hallas, C. R. Wiebe, A. M. Arevalo-Lopez, J. P. Attfield, J. S. Gardner, R. S. Freitas, H. D. Zhou, and J.-G. Cheng, Long-range antiferromagnetic order in the frustrated *XY* pyrochlore antiferromagnet $Er_2Ge_2O_7$, Phys. Rev. B **89**, 064409 (2014).

[46] S. Gao, A. F. May, M.-H. Du, J. A. M. Paddison, H. S. Arachchige, G. Pokharel, C. dela Cruz, Q. Zhang, G. Ehlers, D. S. Parker, D. G. Mandrus, M. B. Stone, and A. D. Christianson, Hierarchical excitations from correlated spin tetrahedra on the breathing pyrochlore lattice, Phys. Rev. B **103**, 214418 (2021).

[47] Z. Y. Zhao, S. Calder, A. A. Aczel, M. A. McGuire, B. C. Sales, D. G. Mandrus, G. Chen, N. Trivedi, H. D. Zhou, and J.-Q. Yan, Fragile singlet ground-state magnetism in the pyrochlore osmates $R_2Os_2O_7$ (R = Y and Ho), Phys. Rev. B **93**, 134426 (2016).

[48] C. M. Pasco, B. A. Trump, T. T. Tran, Z. A. Kelly, C. Hoffmann, I. Heinmaa, R. Stern, and T. M. McQueen, Single-crystal growth of $Cu_4(OH)_6BrF$ and universal behavior in quantum spin liquid candidates synthetic barlowite and herbertsmithite, Phys. Rev. Mater. **2**, 044406 (2018).

[49] P. Malavi, S. Pal, D. V. S. Muthu, S. Sahoo, S. Karmakar, and A. K. Sood, Pressure-induced tuning of quantum spin liquid state in $ZnCu_3(OH)_6Cl_2$, Phys. Rev. B **101**, 214402 (2020).

[50] A. Zorko, M. Herak, M. Gomilšek, J. van Tol, M. Velázquez, P. Khuntia, F. Bert, and P. Mendels, Symmetry reduction in the quantum kagome antiferromagnet herbertsmithite, Phys. Rev. Lett. **118**, 017202 (2017).

[51] R. W. Smaha, I. Boukahil, C. J. Titus, J. M. Jiang, J. P. Sheckelton, W. He, J. Wen, J. Vinson, S. G. Wang, Y.-S. Chen, S. J. Teat, T. P. Devereaux, C. Das Pemmaraju, and Y. S. Lee, Site-specific structure at multiple length scales in kagome quantum spin liquid candidates, Phys. Rev. Mater. **4**, 124406 (2020).

[52] D. P. Shoemaker, R. Seshadri, M. Tachibana, and A. L. Hector, Incoherent Bi off-centering in $Bi_2Ti_2O_6O'$ and $Bi_2Ru_2O_6O'$: Insulator versus metal, Phys. Rev. B **84**, 064117 (2011).

[53] E. S. Bozin, M. Abeykoon, S. Conradson, G. Baldinozzi, P. Sutar, and D. Mihailovic, Crystallization of polarons through charge and spin ordering transitions in 1T-TaS_2, Nat. Commun. **14**, 7055 (2023).

[54] J. Rodríguez-Carvajal, Recent advances in magnetic structure determination by neutron powder diffraction, Phys. B: Condens. Matter **192**, 55 (1993).

[55] B. H. Toby and R. B. Von Dreele, *GSAS*-II: The genesis of a modern open-source all purpose crystallography software package, J. Appl. Cryst. **46**, 544 (2013).

[56] Z. L. Dun, M. Lee, E. S. Choi, A. M. Hallas, C. R. Wiebe, J. S. Gardner, E. Arrighi, R. S. Freitas, A. M. Arevalo-Lopez, J. P. Attfield, H. D. Zhou, and J. G. Cheng, Chemical pressure effects on magnetism in the quantum spin liquid candidates $Yb_2X_2O_7$ (X = Sn, Ti, Ge), Phys. Rev. B **89**, 064401 (2014).

[57] Z. L. Dun, X. Li, R. S. Freitas, E. Arrighi, C. R. Dela Cruz, M. Lee, E. S. Choi, H. B. Cao, H. J. Silverstein, C. R. Wiebe, J. G. Cheng, and H. D. Zhou, Antiferromagnetic order in the

pyrochlores $R_2Ge_2O_7$ (R = Er, Yb), Phys. Rev. B **92**, 140407(R) (2015).

[58] A. M. Hallas, J. Gaudet, M. N. Wilson, T. J. Munsie, A. A. Aczel, M. B. Stone, R. S. Freitas, A. M. Arevalo-Lopez, J. P. Attfield, M. Tachibana, C. R. Wiebe, G. M. Luke, and B. D. Gaulin, XY antiferromagnetic ground state in the effective $S = \frac{1}{2}$ pyrochlore $Yb_2Ge_2O_7$, Phys. Rev. B **93**, 104405 (2016).

[59] See Supplemental Material at http://link.aps.org/supplemental/10.1103/PhysRevB.109.144407 for the frequency dependent ac data, the technical details about the reverse Monte Carlo modeling, and the statistical distribution plots for the various triplet angles.

[60] A. W. C. Wong, Z. Hao, and M. J. P. Gingras, Ground state phase diagram of generic XY pyrochlore magnets with quantum fluctuations, Phys. Rev. B **88**, 144402 (2013).

[61] M. Taillefumier, O. Benton, H. Yan, L. D. C. Jaubert, and N. Shannon, Competing spin liquids and hidden spin-nematic order in spin ice with frustrated transverse exchange, Phys. Rev. X **7**, 041057 (2017).

[62] Y. Zhang, M. Eremenko, V. Krayzman, M. G. Tucker, and I. Levin, New capabilities for enhancement of *RMC*Profile: instrumental profiles with arbitrary peak shapes for structural refinements using the reverse Monte Carlo method, J. Appl. Crystallogr. **53**, 1509 (2020).

[63] M. G. Tucker, D. A. Keen, M. T. Dove, A. L. Goodwin, and Q. Hui, *RMC*profile: reverse Monte Carlo for polycrystalline materials, J. Phys.: Condens. Matter **19**, 335218 (2007).

[64] Data pre-processing for RMCprofile, https://rmcprofile.ornl.gov/data-pre-processing-for-rmcprofile/, accessed: 2023-09-04.

[65] O. Arnold, J. Bilheux, J. Borreguero, A. Buts, S. Campbell, L. Chapon, M. Doucet, N. Draper, R. F. Leal, M. Gigg, V. Lynch, A. Markvardsen, D. Mikkelson, R. Mikkelson, R. Miller, K. Palmen, P. Parker, G. Passos, T. Perring, P. Peterson *et al.*, Mantid-data analysis and visualization package for neutron scattering and μSR experiments, Nucl. Instrum. Methods Phys. Res., Sect. A **764**, 156 (2014).

[66] L. Pan, S. K. Kim, A. Ghosh, C. M. Morris, K. A. Ross, E. Kermarrec, B. D. Gaulin, S. M. Koohpayeh, O. Tchernyshyov, and N. P. Armitage, Low-energy electrodynamics of novel spin excitations in the quantum spin ice $Yb_2Ti_2O_7$, Nat. Commun. **5**, 4970 (2014).

[67] H. Yan, O. Benton, L. Jaubert, and N. Shannon, Theory of multiple-phase competition in pyrochlore magnets with anisotropic exchange with application to $Yb_2Ti_2O_7$, $Er_2Ti_2O_7$, and $Er_2Sn_2O_7$, Phys. Rev. B **95**, 094422 (2017).

[68] J. D. Thompson, P. A. McClarty, H. M. Rønnow, L. P. Regnault, A. Sorge, and M. J. P. Gingras, Rods of neutron scattering intensity in $Yb_2Ti_2O_7$: Compelling evidence for significant anisotropic exchange in a magnetic pyrochlore oxide, Phys. Rev. Lett. **106**, 187202 (2011).

[69] J. Cheng, J. Zhou, R. Hu, W. Xu, Y. Li, L. Zhang, A. Marcelli, W. Chu, Z. an Xu, and Z. Wu, Charge redistribution and local lattice structure of (F, Zn)-codoped LaFeAsO superconductor, New J. Phys. **14**, 033005 (2012).

[70] A. Choi, T. Kim, M.-H. Kim, S. W. Lee, Y. H. Jung, and H.-W. Lee, Mitigating Jahn-Teller effects by fast electrode kinetics inducing charge redistribution, Adv. Funct. Mater. **32**, 2111901 (2022).

[71] M. Maschek, X. You, M. F. J. Boeije, D. Chernyshov, N. H. van Dijk, and E. Brück, Charge redistribution and the magnetoelastic transition across the first-order magnetic transition in $(Mn,Fe)_2(P,Si,B)$, Phys. Rev. B **98**, 224413 (2018).

[72] J. Zhu, L. Yang, H.-W. Wang, J. Zhang, W. Yang, X. Hong, C. Jin, and Y. Zhao, Local structural distortion and electrical transport properties of $Bi(Ni_{1/2}Ti_{1/2})O_3$ perovskite under high pressure, Sci. Rep. **5**, 18229 (2015).